

Spin Current Through a Magnetic-Oscillating Quantum Dot

Ping Zhang^{1,2}, Qi-Kun Xue¹, and X.C. Xie^{1,2}

¹*International Center for Quantum Structures, Institute of Physics,*

Chinese Academy of Sciences, Beijing 100080, P.R. China

²*Department of Physics, Oklahoma State University, Stillwater, OK 74075*

Abstract

Non-equilibrium spin transport through an interacting quantum dot is analyzed. The coherent spin oscillations in the dot provide a generating source for spin current. In the interacting regime, the Kondo effect is influenced in a significant way by the presence of the precessing magnetic field. In particular, when the precession frequency is tuned to resonance between spin up and spin down states of the dot, Kondo singularity for each spin splits into a superposition of two resonance peaks. The Kondo-type cotunneling contribution is manifested by a large enhancement of the pumped spin current in the strong coupling, low temperature regime.

PACS numbers: 72.25.-b, 85.35.Be, 73.23.-b, 03.67.Lx

Key words: Spintronics, quantum dot, Kondo effect

Introduction.—The rapid progress of nano-electronics and information technologies has prompted intense interest in exploiting the interplay of electron charge and spin properties, which results in the emergence of semiconductor spintronics[1, 2]. Since it is a manageable task to manipulate and measure electron and nuclear spins via optical or electric field[3], the solid-state implementation of a quantum information processing architecture is intensely studied[4], aiming at the possibility of large-scalability of the quantum computer. One of the most important spin-based electronic devices is a mesoscopic quantum dot (QD) system, in which the spin coherence time for electrons or nuclei is relatively long[5, 6]. Spin-polarized transport through a QD has been extensively investigated recently. It has been shown theoretically[7, 8] and demonstrated experimentally[9] that a QD system will function as a phase-coherent spin pump in the presence of sizable Zeeman splitting. A QD-based spin battery device has been proposed by use of a combination of a vertical magnetic field and an oscillating electric field[10]. Very recently, spin-polarized current has been detected from a quantum point contact (QPC)[11] and from Coulomb-blockaded QDs[12]. For the latter, due to the large charging energy at low temperatures, a more subtle effect—the creation of new states of many-body character at the Fermi level by the Kondo effect—is expected to occur[13]. Although the effect of Kondo resonance on the charge current has been well studied in a QD[14], its influence on the spin current and spin detection might be equally significant, since it provides a spin-flip cotunneling mechanism.

In this paper we explore spin current response to a magnetic-oscillating quantum dot, which is schematically shown in Fig. 1. The setup is similar to the one used in recent ESR-STM experiments[15]. The single-electron levels in the dot are split by an external magnetic field B_0 , $\varepsilon_{d\downarrow} - \varepsilon_{d\uparrow} = g\mu_B B_0$, where g is the effective electron gyromagnetic factor and μ_B is the Bohr magneton. The two spin levels are coupled by a rotating magnetic field ($B_1 \cos \omega t$, $B_1 \sin \omega t$), applied perpendicularly to the field B_0 . The possibility of the ESR setup based on GaAs QD has been discussed in Ref.[9]. The QD is in some sense similar to an oscillating magnetic dipole moment of a two-level atom. However, we show that the spin transport properties are highly non-trivial for the QD system, due to the many-body excitations and coupling with an external electrode.

Theoretical formalism.—The model Hamiltonian under consideration can be written as

$$\begin{aligned}
H = & \sum_{\sigma} \varepsilon_{d\sigma} d_{\sigma}^{+} d_{\sigma} + U d_{\uparrow}^{+} d_{\uparrow} d_{\downarrow}^{+} d_{\downarrow} - g \mu_B B_1 (d_{\uparrow}^{+} d_{\downarrow} e^{i\omega t} + d_{\downarrow}^{+} d_{\uparrow} e^{-i\omega t}) \\
& + \sum_{k\sigma} \epsilon_{k\sigma} a_{k\sigma}^{+} a_{k\sigma} + \sum_{k\sigma} [V_k a_{k\sigma}^{+} d_{\sigma} + \text{H.c.}].
\end{aligned} \tag{1}$$

Here d_{σ}^{+} and $a_{k\sigma}^{+}$ create an electron of spin σ in the QD and in the lead, respectively. The first two terms in (1) represent correlated spin levels of the QD, the time-dependent terms describe the coupling between two QD spin states $|\uparrow\rangle$ and $|\downarrow\rangle$ by the rotating magnetic field, and the last term is the hybridization of the QD to the lead. A similar model has been proposed for electrical detection of single-electron spin resonance[17, 18].

The time dependence of the Hamiltonian (1) may be eliminated by introducing a unitary transformation $U = e^{-i\frac{\omega t}{2}[\sum_k (a_{k\downarrow}^{+} a_{k\downarrow} - a_{k\uparrow}^{+} a_{k\uparrow}) + (d_{\downarrow}^{+} d_{\downarrow} - d_{\uparrow}^{+} d_{\uparrow})]}$ (\hbar is set to be unity) and thus redefining the Hamiltonian in the rotating reference (RF) as follows

$$\begin{aligned}
H_{RF} = & U^{-1} H U + i \frac{dU^{-1}}{dt} U \\
= & \sum_{\sigma} \tilde{\varepsilon}_{d\sigma} d_{\sigma}^{+} d_{\sigma} + U d_{\uparrow}^{+} d_{\uparrow} d_{\downarrow}^{+} d_{\downarrow} - g \mu_B B_1 (d_{\uparrow}^{+} d_{\downarrow} + d_{\downarrow}^{+} d_{\uparrow}) \\
& + \sum_{k\sigma} \epsilon_{k\sigma} a_{k\sigma}^{+} a_{k\sigma} + \sum_{k\sigma} [V_k a_{k\sigma}^{+} d_{\sigma} + \text{H.c.}],
\end{aligned} \tag{2}$$

where $\tilde{\varepsilon}_{d\sigma} = \varepsilon_{d\sigma} \pm \frac{\omega}{2}$ and $\epsilon_{k\sigma} = \epsilon_k \pm \frac{\omega}{2}$ are the dressed dot and lead levels for up and down spins, respectively. One can see that the rotating magnetic field, in effect, shifts lead electron energy to the opposite directions for up and down spins. This spin-oriented energy splitting originates from the hybridization term in (2), which propagates energy from the QD to the lead. Thus the spin-up chemical potential is now $\mu_{\uparrow} = -\omega/2$ (The reference energy is set $E_F = 0$), while the spin-down chemical potential is $\mu_{\downarrow} = \omega/2$. The charge chemical potential is still $\mu_e = (\mu_{\uparrow} + \mu_{\downarrow})/2 = 0$. The distinction between μ_{σ} and μ_e was recently discussed in Ref.[19].

The physical picture of spin current generation is as follows. Due to the one-photon difference between the spin-down and spin-up chemical potentials of the lead, an electron in the spin-down channel can tunnel into the $\tilde{\varepsilon}_{d\downarrow}$ level in QD. After a spin-flip process given by B_1 term in (2), the electron can tunnel out of the QD into the spin-up channel. This process repeats, so a steady spin current builds up in the lead. Note that the net charge current is zero because there is only one electrode in the system. This zero charge current feature is

retained when more electrodes are taken into account with no bias voltage applied between them. We emphasize that the present situation is not a simple realization of magnetization of the electrode by the rotating magnetic field. Here the generation of spin current is due to real charge transfer processes between the two spin channels of the lead. Therefore, the spin current can be conveniently controlled in experiments. To calculate the spin current we make use of the non-equilibrium Green function formalism.

In the absence of hybridization and Coulomb interaction, the QD is reduced to a simple driven two-level system (TLS). Its dynamics is featured by a coherent weight transfer (Rabi oscillations) between the two spin states, which is complete when the rotating frequency is tuned to the resonant condition $\omega_R = g\mu_B B_0$. The spin oscillation period is $T = \pi/\Omega$, where $\Omega = \sqrt{\Delta^2 + 4(g\mu_B B_1)^2}$ is the Rabi frequency and $\Delta = \omega_R - \omega$ denotes the detuning from the resonance.

To proceed we introduce a canonical transformation

$$\begin{pmatrix} d_\uparrow \\ d_\downarrow \end{pmatrix} = \mathbf{u} \begin{pmatrix} c_\uparrow \\ c_\downarrow \end{pmatrix} \text{ with } \mathbf{u} = \begin{pmatrix} \cos \phi & -\sin \phi \\ \sin \phi & \cos \phi \end{pmatrix}, \quad (3)$$

where $\phi = \tan^{-1}(\frac{2g\mu_B B_1}{\Omega - \Delta})$. In terms of new fermion operators, the dot Hamiltonian in Eq. (2) is has a diagonal form $\sum_\sigma \varepsilon_{c\sigma} c_\sigma^+ c_\sigma + U c_\uparrow^+ c_\uparrow c_\downarrow^+ c_\downarrow$ with $\varepsilon_{c\sigma} = (\varepsilon_{d\uparrow} + \varepsilon_{d\downarrow} \pm \Omega)/2$ for the up and down spins.

The spin- σ , say spin- \uparrow , current can be calculated from the time evolution of the occupation number $N_\uparrow(t) = \sum_k c_{k\uparrow}^+ c_{k\uparrow}$ for electrons in the electrode using the non-equilibrium Green function:

$$J_\uparrow = -e \frac{d}{dt} \langle N_\uparrow(t) \rangle = \frac{2e}{\hbar} \text{Re} \left\{ \sum_k V_k \int \frac{d\epsilon}{2\pi} [\mathbf{u} \mathbf{G}_{k,c}^<(\epsilon)]_{\uparrow\uparrow} \right\}, \quad (4)$$

where we have defined the lesser Green function matrix $[\mathbf{G}_{k,c}^<(t)]_{\sigma\sigma'} = i \langle c_{\sigma'}^+(0) a_{k\sigma}(t) \rangle$. Next, we use Dyson's equation to calculate $\mathbf{G}_{k,c}^<$ and express J_\uparrow by the Green functions of the dot as follows

$$J_\uparrow = \frac{ie}{\hbar} \int \frac{d\epsilon}{2\pi} \Gamma(\epsilon) \left(\mathbf{u} \{ \mathbf{G}_c^<(\epsilon) + f_\uparrow(\epsilon) [\mathbf{G}_c^r(\epsilon) - \mathbf{G}_c^a(\epsilon)] \} \mathbf{u}^T \right)_{\uparrow\uparrow}, \quad (5)$$

where $\Gamma(\epsilon) = 2\pi \sum_k |V_k|^2 \delta(\epsilon - \epsilon_k)$ and $[\mathbf{G}_c^<(t)]_{\sigma\sigma'} = i \langle c_{\sigma'}^+(0) c_\sigma(t) \rangle$ are the lesser Green functions of the dot, $\mathbf{A} = \mathbf{G}_c^r - \mathbf{G}_c^a$ is the spectral function matrix, and $f_\sigma(\epsilon) = f(\epsilon - \mu_\sigma)$ are the Fermi distribution functions for the spin-up and spin-down channels.

The non-interacting spin current.—In the non-interacting ($U = 0$) case or within the mean field (MF) treatment of the Coulomb interaction for finite U , the retarded Green

function matrix is given by

$$[\mathbf{G}_c^r(\epsilon)]_{\sigma\sigma'} = \delta_{\sigma\sigma'} \frac{1}{[\mathbf{g}_c^{r-1}(\epsilon)]_{\sigma\sigma} - [\Sigma_0^r(\epsilon)]_{\sigma\sigma}}, \quad (6)$$

where $\Sigma_0^r = -i\Gamma\mathbf{I}$ is the tunneling contribution to the retarded self-energy, and $\mathbf{g}_c^r(\epsilon)$ is the unperturbed Green function matrix of the dot, which in the mean-field approximation has a simple Hartree-Fock type $[\mathbf{g}^R(\epsilon)]_{\sigma\sigma'} = \delta_{\sigma\sigma'} [\frac{n_{c\sigma}}{\epsilon - \epsilon_{c\sigma} - U} + \frac{1 - n_{c\sigma}}{\epsilon - \epsilon_{c\sigma}}]$ with $n_{c\sigma} = \langle c_\sigma^+ c_\sigma \rangle$. $n_{c\sigma}$ must be calculated self-consistently via the relation $n_{c\sigma} = \text{Im} \int \frac{d\epsilon}{2\pi} [\mathbf{G}_c^<(\epsilon)]_{\sigma\sigma}$. The lesser Green functions in (5) are obtained via the Keldysh equation $\mathbf{G}_c^< = \mathbf{G}_c^r \Sigma_0^< \mathbf{G}_c^a$ with the lesser self-energy matrix

$$\Sigma_0^< = i\Gamma \begin{pmatrix} f_\uparrow(\epsilon) \cos^2 \phi + f_\downarrow(\epsilon) \sin^2 \phi & \sin \phi \cos \phi [f_\downarrow(\epsilon) - f_\uparrow(\epsilon)] \\ \sin \phi \cos \phi [f_\downarrow(\epsilon) - f_\uparrow(\epsilon)] & f_\uparrow(\epsilon) \sin^2 \phi + f_\downarrow(\epsilon) \cos^2 \phi \end{pmatrix}. \quad (7)$$

Substituting the expressions for $\mathbf{G}_c^<$ into (5), we obtain the expression for the tunneling spin current

$$J_\uparrow = \frac{e\Gamma}{\hbar} \int \frac{d\epsilon}{2\pi} \{ \mathbf{u} \mathbf{G}_0^r(\epsilon) \bar{\Sigma}_0^< \mathbf{G}_0^a(\epsilon) \mathbf{u}^T \}_{\uparrow\uparrow} \{ f_\uparrow(\epsilon) - f_\downarrow(\epsilon) \}, \quad (8)$$

where

$$\bar{\Sigma}_0^< = \Gamma \begin{pmatrix} \sin^2 \phi & \sin \phi \cos \phi \\ \sin \phi \cos \phi & \cos^2 \phi \end{pmatrix}. \quad (9)$$

Since the electrons are flowing from spin-down channel to spin-up channel, we define the total spin current as $J_s = J_\downarrow - J_\uparrow = -2J_\uparrow$. Although the coherent spin superposition is strongest at two-level resonance $\omega = \omega_R$, the spin current is also influenced by the spin levels $\tilde{\varepsilon}_{d\sigma}$ relative to μ_σ . Figure 2(a) shows the non-interacting spin current versus rotating frequency at different temperatures. The undressed spin levels are set to lie deeply below E_F . One can see that at low temperature (solid line), the spin current peak is not at, but far from $\omega = \omega_R$. This is because at $\omega = \omega_R$ the dressed spin-up level $\tilde{\varepsilon}_{d\uparrow}$ is still lower than μ_\uparrow and thus the electron in the dot cannot tunnel out via small thermal excitation. Due to the state exchange in QD, as shown in the inset of Fig. 2(a), when ω increases further, crossing the avoided crossing between the two spin levels, the upper eigenstate is dominated by spin component $|\uparrow\rangle$ while the lower state by $|\downarrow\rangle$. Thus when the upper level is higher than μ_\uparrow , spin tunneling processes occurs, and a peak develops in the current spectrum. When the temperature is increased to $k_B T \sim |\mu_\uparrow - \tilde{\varepsilon}_{d\uparrow}|$, the spin-current peak shifts to $\omega = \omega_R$ with a larger peak amplitude. Further increasing temperature such that $k_B T > \omega$ will smear out

the mismatch between μ_\uparrow and μ_\downarrow , and thus the spin current amplitude begins to decrease, as shown in Fig. 2(a). The dot levels can be conveniently controlled by the gate voltage V_g . When V_g is modulated such that $\tilde{\varepsilon}_{d\sigma}$ are at the interval between μ_\downarrow and μ_\uparrow , then the spin current peak will occur exactly at $\omega = \omega_R$ [see Fig. 2(b)].

The model can also illustrate the spin-current generation in the Coulomb blockade regime when Coulomb interaction U is treated in the mean-field formalism. As an example, we show in Fig. 3 the spin current versus gate voltage for several values of ω . Two Coulomb peaks with interval U can be resolved, and as in Fig. 2, the current amplitude increases when the magnetic field frequency is tuned towards to two-level resonance $\omega = \omega_R$.

The electronic correlation effect.—In the low temperature, strong coupling, and large charging energy regime, correlation effects enter and are expected to significantly influence the spin transport. To illustrate correlation effects, we again use the equation of motion method to solve the retarded Green function in (2), which generates higher-order Green functions that have to be truncated to close the equation[20]. After a straightforward calculation, in the infinite- U limit we obtain

$$\mathbf{G}^r(\epsilon) = [\epsilon \mathbf{I} - \widehat{\tilde{\varepsilon}}_d - \Sigma_0^r(\epsilon) - \Sigma_1^r(\epsilon)]^{-1}(\mathbf{I} - \mathbf{n}_c), \quad (10)$$

where $(\widehat{\tilde{\varepsilon}}_d)_{\sigma\sigma'} = \delta_{\sigma\sigma'} \tilde{\varepsilon}_{d\sigma}$ and the interaction self-energies are given by $[\Sigma_1^r(\epsilon)]_{\sigma\sigma'} = \delta_{\sigma\sigma'} \sum_k [\frac{\sin^2 \phi |V_k|^2 f(\epsilon_{k\sigma})}{\epsilon - \epsilon_{k\sigma} - \varepsilon_{c\sigma} + \varepsilon_{c\sigma}} + \frac{\cos^2 \phi |V_k|^2 f(\epsilon_{k\sigma})}{\epsilon - \epsilon_{k\sigma} - \varepsilon_{c\sigma} + \varepsilon_{c\sigma}}]$. $(\mathbf{n}_c)_{\sigma\sigma'} = \delta_{\sigma\sigma'} \langle c_\sigma^+ c_{\sigma'}^- \rangle$ needs to be calculated self-consistently via the relation $\langle c_\sigma^+ c_\sigma^- \rangle = \text{Im} \int \frac{d\epsilon}{2\pi} \mathbf{G}_{\sigma\sigma}^<(\epsilon)$. $\mathbf{G}^<(\epsilon)$ is difficult to obtain since the lesser self-energy cannot be given exactly in the interacting regime. However, the situation simplifies in the steady-state transport[21], in which the occupation on the dot is time-independent, $i \frac{d}{dt} \langle c_\sigma^+(t) c_\sigma^-(t) \rangle = 0$. Writing down the Heisenberg equations for $c_\sigma^+(t)$ and $c_\sigma^-(t)$, and integrating out the lead electron operators, we find the self-consistent integral equations for the retarded Green functions as follows:

$$\langle c_\uparrow^+ c_\uparrow^- \rangle = \text{Im} \int \frac{d\epsilon}{2\pi} \mathbf{G}_{\uparrow\uparrow}^<(\epsilon) = \int \frac{d\epsilon}{2\pi} \text{Im}(\mathbf{G}_{\uparrow\uparrow}^a - \mathbf{G}_{\uparrow\uparrow}^r) [\cos^2 \phi f_\uparrow + \sin^2 \phi f_\downarrow], \quad (11a)$$

$$\langle c_\downarrow^+ c_\downarrow^- \rangle = \text{Im} \int \frac{d\epsilon}{2\pi} \mathbf{G}_{\downarrow\downarrow}^<(\epsilon) = \int \frac{d\epsilon}{2\pi} \text{Im}(\mathbf{G}_{\downarrow\downarrow}^a - \mathbf{G}_{\downarrow\downarrow}^r) [\sin^2 \phi f_\uparrow(\epsilon) + \cos^2 \phi f_\downarrow(\epsilon)], \quad (11b)$$

which now, together with (10), close the equations of motion for \mathbf{G}^r . Similarly, the quantities $\langle c_\sigma^+ c_{\sigma'}^- \rangle = -i \int \frac{d\epsilon}{2\pi} G_{\sigma\sigma'}^<(\epsilon)$ can also be expressed by the retarded Green functions. Thus we can calculate the spin current in (5) directly after $\mathbf{G}^r(\epsilon)$ is numerically obtained.

The magnetic-field-induced excitation properties are shown in Fig. 4 by plotting local spin-resolved spectral densities $\rho_\sigma(\epsilon) = [\mathbf{u}\mathbf{G}_c^r(\epsilon)\mathbf{u}^T]_{\sigma\sigma}$ for different values of ω . In the absence of a rotating magnetic field ($\omega, B_1 = 0$), as observed from Fig. 4(a), the spectral density for each spin component is characterized by a broad single-particle peak around $\varepsilon_{d\sigma}$, and a sharp Kondo peak at Zeeman energies $\epsilon = -\omega_R$ for up spin and $\epsilon = \omega_R$ for down spin. The spectral weight of ρ_\uparrow is enhanced by the magnetic field, while ρ_\downarrow is greatly suppressed. Therefore, a net spin moment develops in the QD. Physically, the Kondo peak at $\epsilon = -\omega_R$ is due to the cotunneling processes (see inset) in which one spin-down electron in the lead at the Fermi level tunnels into the dot and occupies energy level $\tilde{\varepsilon}_\downarrow$, followed by another electron on $\tilde{\varepsilon}_\uparrow$ tunneling out to the spin-up channel with the energy ω_R below from Fermi level E_F . Such cotunneling processes transfer electrons from spin-up channel to spin-down channel of the lead. Thus *a spin current may be induced in an efficient way by these Kondo-type cotunneling processes*. Similarly, the Kondo peak at $\epsilon = \omega_R$ in $\rho_\downarrow(\epsilon)$ is due to a superposition of many cotunneling processes in which one spin down electron with the energy ω_R above the Fermi level tunnels into the dot and simultaneously another spin-up electron in the dot tunnels out to the Fermi level of the lead. Both kinds of cotunneling processes contribute to the spin-current generation. When the rotating magnetic field is switched on, the spin Kondo resonances and spectral structures begin to change. At $\omega < \omega_R$, the broad single-spin and sharp Kondo peaks shift toward higher energies for up spin, while they shift to lower energies for down spin [Fig. 4(b)]. At two-level resonance $\omega = \omega_R$, as shown in Fig. 4(c): (i) each spin Kondo singularity splits into two prominent peaks around μ_\uparrow and μ_\downarrow ; (ii) $\rho_\uparrow(\epsilon)$ and $\rho_\downarrow(\epsilon)$ completely overlap with identical spectral weight. This overlap is caused by the fact that at $\omega = \omega_R$, each spin eigenstate in the dot is a strong superposition of $|\uparrow\rangle$ and $|\downarrow\rangle$ states with equal probability amplitude. When ω increases further, the two-level superposition is suppressed, and the state exchange occurs. As a response, the spectral densities of two spins also exchange their structures; as can be seen from Fig. 4(d), $\rho_\downarrow(\epsilon)$ is enhanced while $\rho_\uparrow(\epsilon)$ is greatly suppressed.

To see the influence of the many-body correlation effect on the spin transport, we show in Figure 5 the spin current as a function of rotating frequency. Compared to the non-interacting case, it can be seen that the spin current is greatly enhanced by the cotunneling processes in the strong coupling, low temperature regime. A detailed study of cotunneling effects on the spin current is in progress.

In summary, we have analyzed the spin current properties of an interacting QD exposed to a rotating magnetic field. The spin-flip process in the QD and the effective difference of two spin chemical potentials suffices the generation of spin current with no charge current. The interplay of the many-body cotunneling process and coherent two-level resonance in the QD produces a remarkable enhancement of spin current. Since a controllable generation of spin current provides an efficient source for spin injection, spin detection, and various variety of spin-based devices, we expect the present results may have practical applications in the field of spintronics.

This work was supported by grants CNSF 90103024, MOST-G001CB3095, and U.S.-DOE-DE-FG03-98ER45687.

- [1] S. Datta and B. Das, *Appl. Phys. Lett.* **56**, 665 (1990).
- [2] G. A. Prinz, *Science* **282**, 1660 (1998); S.A. Wolf *et al.*, *Science* **294**, 1488 (2001).
- [3] B. Kane, *Nature* **393**, 133 (1998).
- [4] D.D. Awschalom, N. Sarmarth, and D. Loss, eds., *Semiconductor Spintronics and Quantum Computation* (Springer-Verlag, Berlin, 2002).
- [5] J.M. Kikkawa and D.D. Awschalom, *Phys. Rev. Lett.* **80**, 4313 (1998).
- [6] H. Hanson *et al.*, cond-mat/0303139.
- [7] E.R. Mucciolo, C. Chamon, and C. Marcus, *Phys. Rev. Lett.* **89**, 146802 (2002); T. Aono, cond-mat/0205395.
- [8] B. Wang, J. Wang, and H. Guo, cond-mat/0208475.
- [9] S.K. Watson *et al.*, cond-mat/0302492.
- [10] Q.-F. Sun, H. Guo, and J. Wang, cond-mat/0212293.
- [11] R.M. Potok *et al.*, *Phys. Rev. Lett.* **89**, 266602 (2002).
- [12] R.M. Potok *et al.*, cond-mat/0303152.
- [13] A.C. Hewson, *The Kondo Problem to Heavy Fermions* (Cambridge University Press, Cambridge, England, 1993).
- [14] L. Kouwenhoven and L. Glazman, *Physics World* 14, 33 (2001), and references therein.
- [15] A. Wachowiak *et al.*, *Science* **298**, 577 (2002); A. Kubetzka *et al.*, *Phys. Rev. Lett.* **88**, 057201 (2002).

- [16] L.M.K. Vandersypen *et al.*, quant-ph/0207059.
- [17] H.-A. Engel and D. Loss, Phys. Rev Lett. 86, 4648 (2001).
- [18] I. Martin, D. Mozyrsky, and H.W. Jiang, Phys. Rev. Lett. 90, 018301 (2003).
- [19] M.Y. Veillette, C. Bena, and L. Balents, cond-mat/0212308.
- [20] Y. Meir and N.S. Wingreen, Phys. Rev. Lett. **68**, 2512 (1992).
- [21] Q.-F. Sun and H. Guo, Phys. Rev. B **66**, 155308 (2002).

Figure captions

Fig. 1. Model setup for spin transport through a QD. The degenerate spin levels in the dot are split and coupled by the external magnetic fields B_0 and B_1 , respectively. Due to the imbalance between spin-up and spin-down chemical potentials (see text), the electron tunnels from the spin-down channel, through the QD, to the spin-up channel.

Fig. 2. (a) Non-interacting spin current as a function of rotating frequency at different temperatures with the undressed spin levels set $\varepsilon_{d\uparrow} = -2.5$, $\varepsilon_{d\downarrow} = -1.5$; (b) Contour plot of spin current as a function of gate voltage and rotating frequency. The spin levels in the dot are modulated by the gate voltage as $\varepsilon_{d\sigma}(V_g) = \varepsilon_{d\sigma} + eV_g$ with $\varepsilon_{d\uparrow} = 1$, $\varepsilon_{d\downarrow} = 2$. Other parameters are $\Gamma = 0.1$ and $g\mu_B B_1 = 0.2$.

Fig. 3. Spin current versus gate voltage for different rotating frequencies with $U = 2$. Other parameters are the same as in Fig. 2(b).

Fig. 4. The spin up (solid line) and spin down (dashed line) spectral densities at different rotating frequency. Parameters are $\varepsilon_{d\uparrow} = -2.5\Gamma$, $\varepsilon_{d\downarrow} = -1.5\Gamma$, $T = 0.001\Gamma$, and $g\mu_B B_1 = 0.2\Gamma$.

Fig. 5. Spin current as a function of rotating frequency in the Kondo-type cotunneling regime (solid line). The non-interacting spin current is also shown (dotted line) for comparison. Other parameters are the same as in Fig. 4.

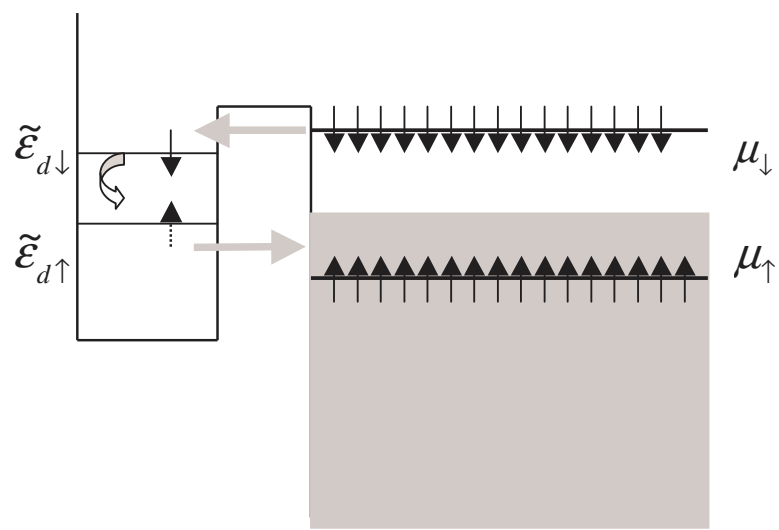


Fig. 1 Zhang et al.

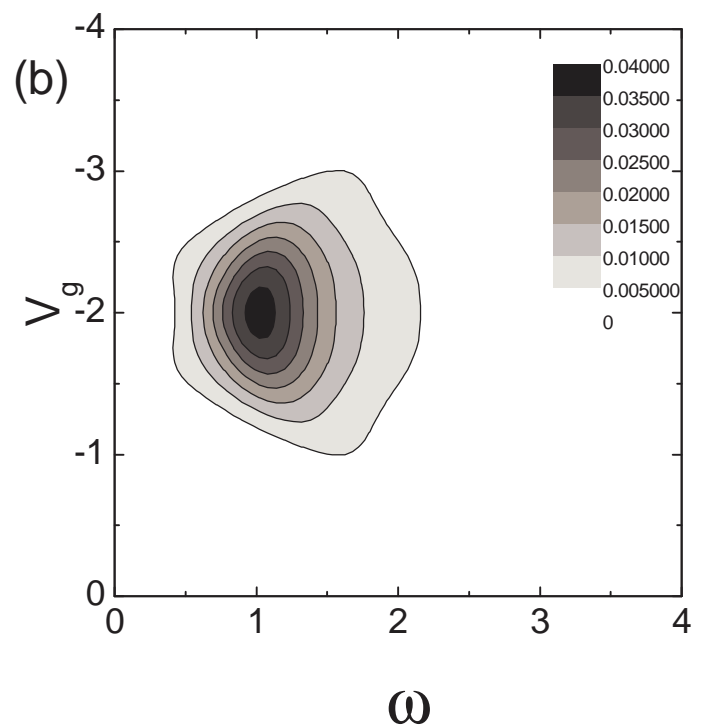
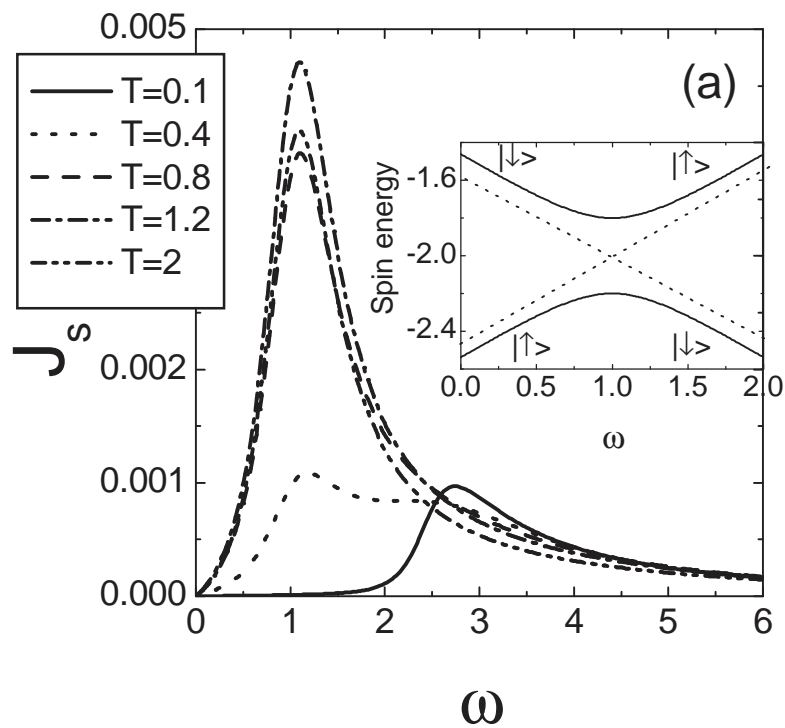


Fig. 2 Zhang et al.

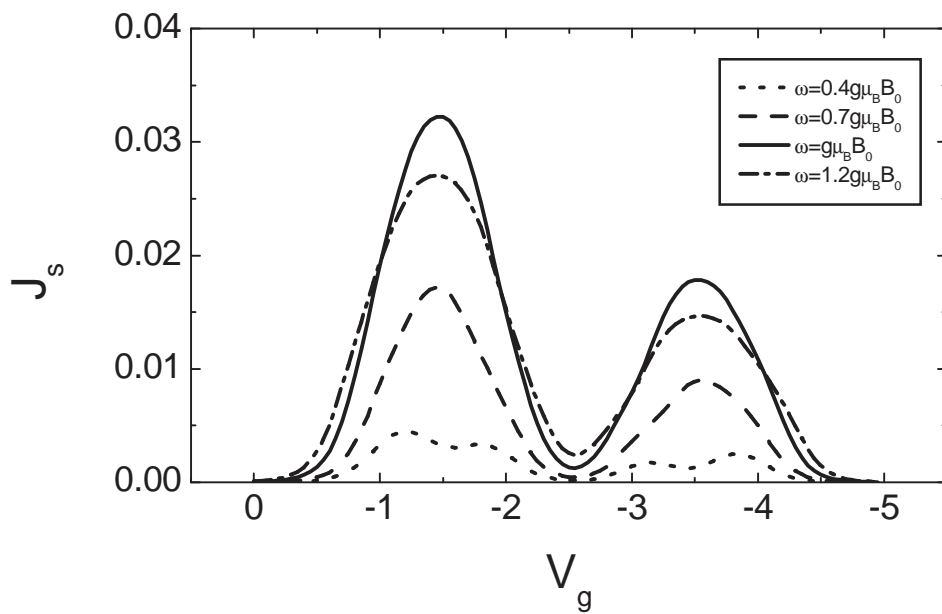


Fig. 3 Zhang et al.

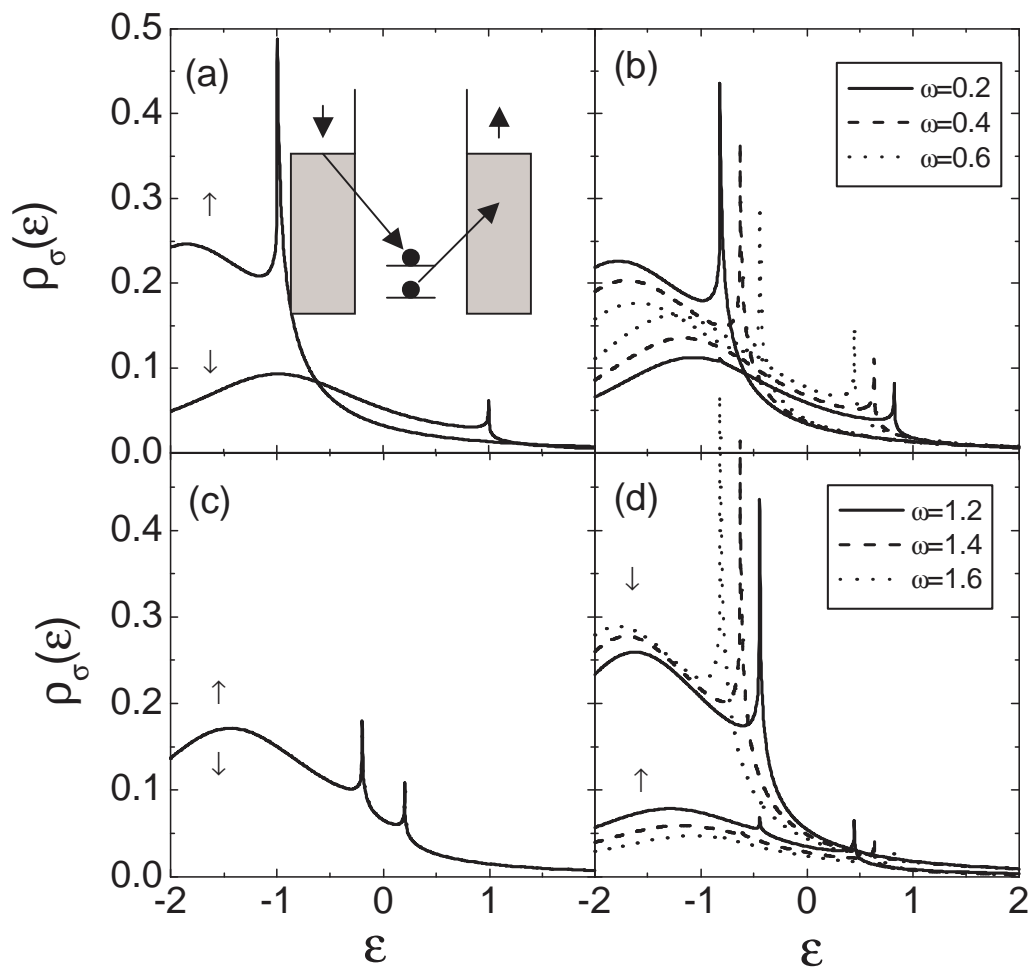


Fig.4 Zhang et al.

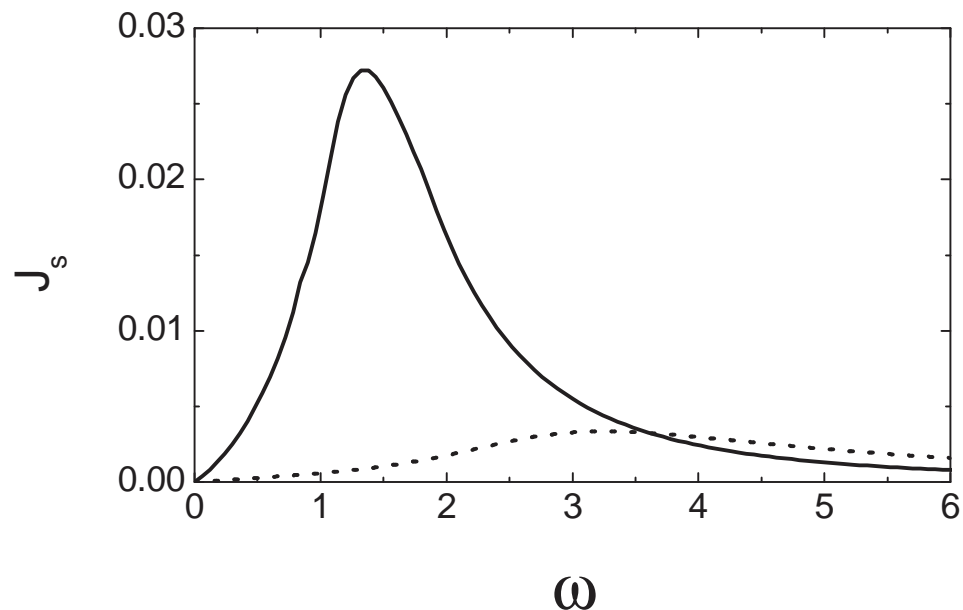


Fig. 5 Zhang et al.